Ultrahigh-bandwidth, on-chip all-optical pulse erasure using the $\chi^{(3)}$ process in a nonlinear chalcogenide waveguide

Ravi Pant,[1,3,*] Trung D. Vo,[1,3] Chunle Xiong,[1,3] Mark D. Pelusi,[1,3] Steve J. Madden,[2,3] Barry Luther-Davies,[2,3] and Benjamin J. Eggleton[1,3]

[1]*Institute of Photonics and Optical Science (IPOS), School of Physics, University of Sydney, Sydney, New South Wales 2006, Australia*

[2]*Laser Physics Centre, Australian National University, Canberra, Australian Capital Territory 0200, Australia*

[3]*Center for Ultrahigh-Bandwidth Devices for Optical Systems (CUDOS), Sydney, Australia*

**Corresponding author: rpant@physics.usyd.edu.au*

Received September 27, 2010; revised November 2, 2010; accepted November 5, 2010; posted November 19, 2010 (Doc. ID 135633); published January 14, 2011

We demonstrate on-chip all-optical pulse erasure based on four-wave mixing and cross-phase modulation in a dispersion engineered chalcogenide (As_2S_3) rib waveguide. We achieve an erasure efficiency of ~15 dB for picosecond pulses in good agreement with numerical simulations using the nonlinear Schrödinger equation. The combined effect of the high instantaneous optical nonlinearity ($\gamma = 9900\,(\mathrm{W\,km})^{-1}$) and small group-velocity dispersion ($D = 29\,\mathrm{ps/nm\,km}$), which reduces pulse walk-off, will enable all-optical pulse erasure for ultrafast signal processing.

OCIS codes: 190.0190, 190.4360, 190.7110.

Ultrafast optical networks are critical for meeting the ever-increasing data demand. In order to realize these ultrafast optical networks, processing data in the optical domain without undergoing optical-to-electrical conversion is necessary. Many of these optical signal processing tasks can be realized using nonlinear optical interactions between light beams, where one light beam is used to control the phase or amplitude of the other optical beam. Optical pulse erasure, where an optical pulse at wavelength λ_1 (channel 1) is erased when it interacts with an optical pulse at wavelength λ_2 (channel 2), is crucial to realize all-optical logic operations such as NOT, XOR gates, demultiplexing, and label swapping [1–7].

Pulse erasure has been investigated in the context of logic gates, demultiplexing, and optical label swapping [1–7]. In these studies, pulse erasure was realized using cross-gain modulation in semiconductor optical amplifiers (SOAs) [3,8]; $\chi^{(2)}$ processes such as cascaded sum/difference frequency generation in periodically poled lithium niobate (PPLN) [5,9]; and $\chi^{(3)}$ nonlinear processes such as four-wave mixing (FWM), cross-phase modulation (XPM), and Raman gain in highly nonlinear fibers (HNLFs) [1,4,7]. While the SOA-based approach is attractive because of its low energy consumption and integration potential, it suffers from bandwidth limitation due to the large gain recovery time ($\tau_{gr} \sim$ tens of picoseconds) [8]. PPLN requires quasi phase matching and temperature stabilization and has limited bandwidth [9,10]. In contrast, pulse erasure exploiting the instantaneous response of $\chi^{(3)}$ nonlinear processes, such as FWM, XPM, or Raman gain, offers inherently ultrahigh operation bandwidth. Although impressive results have been achieved [1,4,7], the HNLF approach is not compatible with integration and has limited bandwidth due to the effect of group-velocity dispersion (GVD), which induces pulse walk-off.

In this Letter, we demonstrate on-chip, all-optical pulse erasure using $\chi^{(3)}$ nonlinear processes in a chalcogenide (As_2S_3) waveguide, which is an attractive platform for nonlinear optical signal processing [11–13]. We exploit XPM and FWM in a dispersion engineered As_2S_3 rib waveguide to achieve 15 dB depletion for picosecond pulses. Measured spectra and pulse shapes show a good agreement with the nonlinear Schrödinger equation (NLSE) simulations. Simulation results for different filter bandwidths were used to analyze the contribution of XPM and FWM to pulse erasure.

Figure 1 summarizes the principle of the all-optical pulse erasure scheme where two channels centered at wavelengths λ_1 and λ_2 copropagate through the nonlinear waveguide and interact via FWM and XPM. The effect of these Kerr nonlinearities combined with the filtering process depletes the power in the input channels, which results in pulse erasure. FWM contributes to erasure by transferring energy from the input channels to generate new frequencies (idlers), as shown in Fig. 1. In contrast, XPM depletes the power in the spectral band of the input channel via the nonlinear phase shift induced spectral broadening and creation of a multipeak structure [14] with spectral holes (see Fig. 1).

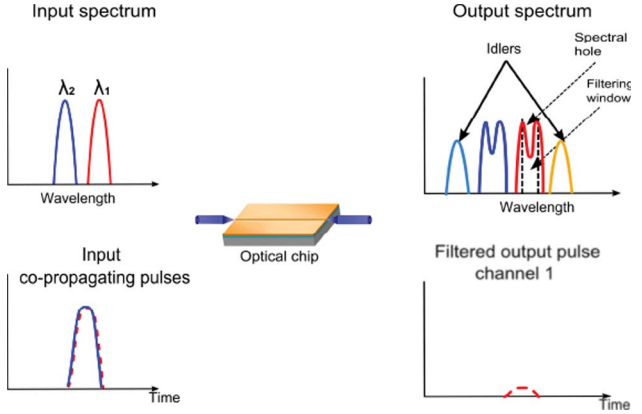

Fig. 1. (Color online) Concept of optical pulse erasure using $\chi^{(3)}$ nonlinear processes when pulses are copropagated.

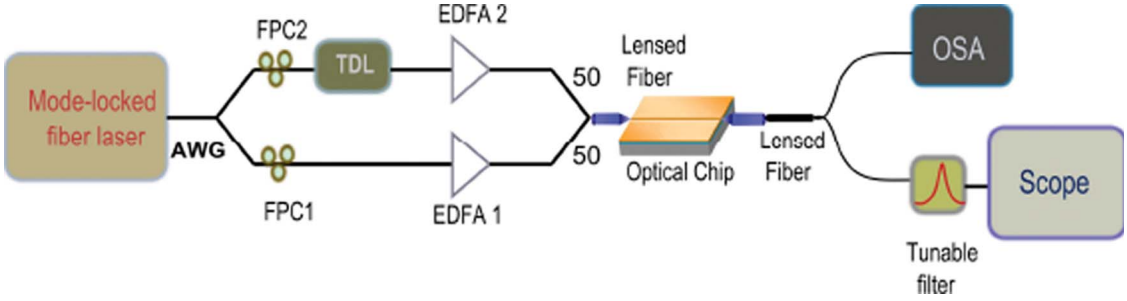

Fig. 2. (Color online) Experimental setup for realizing optical pulse erasure in an As_2S_3 waveguide.

The contribution of the FWM to erasure can be understood from the efficiency (η) of the idler generation, which, under the undepleted pump approximation, depends on the power ($P_{1,2}$) in two channels according to [14]

$$\eta = P_3(L)/P_3(0) = 1 + 2\gamma P_1 P_2 \sinh^2(gL), \qquad (1)$$

where γ is the nonlinear parameter and the parametric gain is $g = (4\gamma^2 P_1 P_2 - \kappa^2(\omega_3)/4)^{1/2}$. The phase mismatch factor κ at the idler frequency ω_3 is $\kappa = \Delta k + \gamma(P_1 + P_2)$ with Δk defined as $\Delta k(\omega_3) = 2\Sigma_{m=1}^{m=\infty}\beta_{2m}[(\omega_3 - \omega_c)^{2m} - \omega_d^{2m}]/(2m!)$, where $\omega_c = (\omega_1 + \omega_2)/2$ and $\omega_d = (\omega_2 - \omega_1)/2$, with ω_1 and ω_2 being the frequency of the input channels. From Eq. (1), it is evident that when both the channels are pulsed, the efficiency of the idler generation depends on the delay between the channels and the peak power of the pulses. Therefore, for the fixed peak power, η is the maximum when the delay is the minimum; in this case, the energy is transferred from the input channels to the idler wavelengths, resulting in erasure. However, depletion of the pump complicates the phase matching, hence we must solve the NLSE to investigate this scheme.

For XPM, the spectral broadening ($d\omega = \Delta\phi_1/T_0$) [14] and multipeak structure occur as a result of the phase shift ($\Delta\phi_1 = 2\gamma_1 P_2 L_w$) induced in channel 1, where P_2 is the peak power in channel 2, γ_1 is the nonlinear coefficient at wavelength λ_1, L_w is the walk-off length, and T_0 is the pulse width. For higher bit rates, pulse spectral broadening therefore increases because T_0 reduces.

Figure 2 shows the experimental setup for realizing pulse erasure. Two channels, 1 and 2, with respective wavelengths 1555 and 1551 nm, are generated by sampling the spectrum of a mode-locked laser, with a 10 MHz repetition rate, using an arrayed waveguide with 0.64 nm bandwidth filters. Fiber polarization controllers (FPCs) are used to align the polarization of the two channels with the TM mode of the waveguide for which the GVD parameter (D) is 29 ps/km nm. A tunable delay line is used in channel 2 to control the delay between the two channels. The pulse power is adjusted using low-noise erbium-doped fiber amplifiers (EDFAs). The amplified pulses are then combined using a 50:50 coupler and launched into the waveguide using a lensed fiber. The peak power in channels 1 and 2 coupled to the waveguide is 4.3 and 3.9 W, respectively. The input pulse width is 7 ps, assuming the Gaussian pulse shape. We use a 7 cm long, dispersion engineered As_2S_3 waveguide with $\gamma = 9900\,(\mathrm{W\,km})^{-1}$ and cross-sectional area of $2\,\mu\mathrm{m} \times 870$ nm. The total insertion loss is ~14 dB, which includes a propagation loss of 0.65 dB/cm. To investigate the pulse erasure, channel 1 is filtered with a 0.64 nm bandwidth filter, the same as is used to generate the two input channels and the output pulse in channel 1 is observed using a 50 Ghz oscilloscope. A portion of the output is directly sent to the optical spectrum analyzer (OSA) to record the full output spectrum.

Figure 3 shows the measured (solid curve) and simulated (dashed curve) channel 1 output pulse normalized using the output power for the maximum delay and

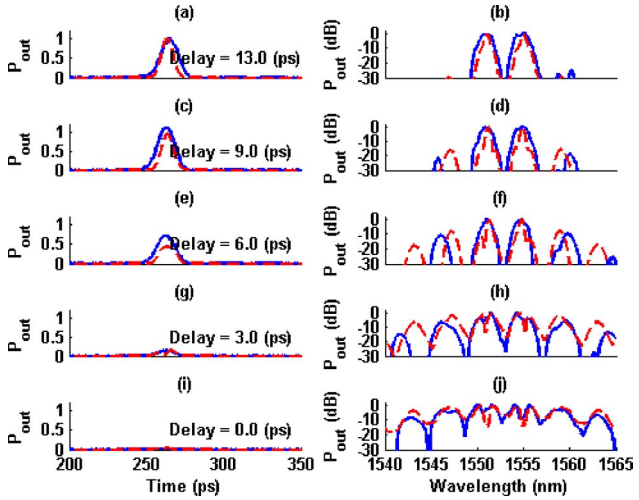

Fig. 3. (Color online) Measured (solid curve) and simulated (dashed curve) channel 1 output pulse normalized using the power for the largest delay and normalized output spectra for different pulse delays between the two channels showing erasure of the channel 1 pulse due to the combined effect of FWM and XPM for the complete overlap.

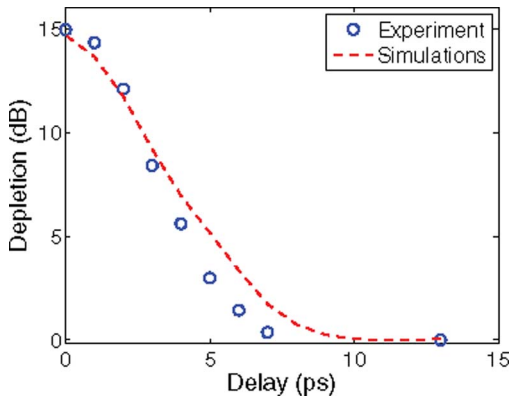

Fig. 4. (Color online) Experimental (circles) and simulated (dashed curve) channel 1 depletion calculated using the expression $-10\log_{10}(P_{\mathrm{out}}(t_{\mathrm{delay}})/P_{\mathrm{out}}(t_{\mathrm{delay}}^{\mathrm{max}}))$ as a function of delay for a 7 ps pulse.

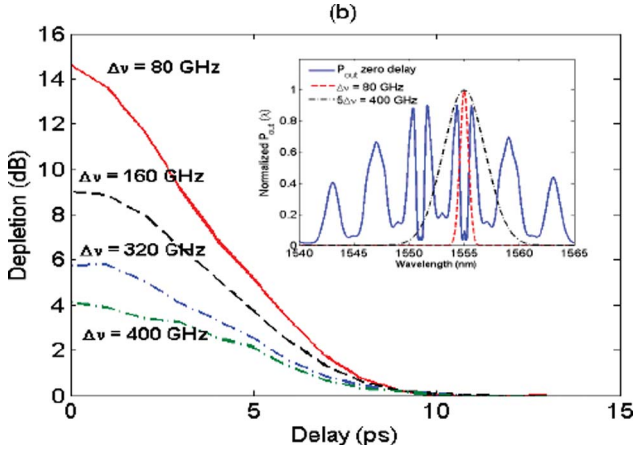

Fig. 5. (Color online) Depletion of a 7 ps pulse as a function of delay for different output filter bandwidths with the inset showing the effect of the filter bandwidth on the output spectrum at a zero delay.

normalized output spectra for five different delays between the pulses in two channels. The simulated output spectra and pulses are generated by solving the NLSE, including the contribution from FWM, XPM/self-phase modulation (SPM) and using the GVD, nonlinear, and absorption parameters for the waveguide. We assume a Gaussian pulse shape and equal coupling loss at the input and output of the waveguide. Although SPM also broadens the pulse spectrum, its contribution is the same for all the delays, and so it has a negligible impact on the pulse erasure. Note that the experimental and simulation results are in good agreement for all the delays. For a large delay between the two channels, very small FWM occurs [see Fig. 3(b)] and the pulse in channel 1 is undepleted [see Fig. 3(a)]. For reduced delay, the pulses start to interact via (i) FWM, which depletes the channels due to idler generation [Figs. 3(a)–3(f)] and (ii) XPM, which broadens the output pulse spectrum and creates a spectral hole at λ_1 [see Figs. 3(g)–3(j)], reducing the energy in the filter passband and completely erasing the pulse in channel 1.

Figure 4 plots the channel 1 depletion for both the experiments and simulations, calculated using the expression $-10\log_{10}(P_{\text{out}}(t_{\text{delay}})/P_{\text{out}}(t_{\text{delay}}^{\max}))$, as a function of delay (t_{delay}) between the pulses in two channels, where $t_{\text{delay}}^{\max}$ is the maximum delay. From Figs. 3 and 4, we note that the experimental results show a good agreement with the NLSE simulations.

In order to analyze the contribution of FWM and XPM to erasure, we repeated the simulations for delays in the range 0–13 ps using different filter bandwidths. Figure 5 plots the channel 1 erasure as a function of delay for filter bandwidths in the range $\Delta\nu$ to $5\Delta\nu$, where $\Delta\nu = 1/T_{\text{pulse}}$. For the filter bandwidth $5\Delta\nu$, the output pulse spectrum completely lies inside the filter band (see inset); therefore, only FWM contributes to depletion. From Fig. 5, we note that the depletion plot for $5\Delta\nu$ contributes ~4 dB to erasure, which is also obvious from Figs. 3(e) and 3(f), where a major contribution to depletion comes from FWM. Thus, XPM adds another 11 dB to depletion, as seen from the plot for the filter bandwidth $\Delta\nu = 80$ GHz.

In conclusion, we have presented highly efficient, on-chip, all-optical pulse erasure based on the $\chi^{(3)}$ nonlinear process for enabling ultrafast signal processing. Pulse depletion of 15 dB is achieved for a 7 ps pulse, which can be further increased by increasing the power, with FWM and XPM contributing ~4 dB and 11 dB, respectively. The major advance offered in our device is dispersion engineering ($D = 29$ ps/km nm), which reduces walk-off for realizing erasure for ultrafast signal processing tasks such as logic operations and demultiplexing. However, the energy required for erasure is 28 pJ, which is larger than that used in SOA (a fraction of a picojoule). The effective mode area can be further reduced by a factor of 5 to 10 times [15] to make the pulse energy of the same order as in SOA; however, better design and fabrication are required to reduce the scattering losses.

This work was supported by the Australian Research Council (ARC) through its ARC Centre of Excellence and Federation Fellowship programs.

References

1. G. Burdge, S. U. Alam, A. Grudinin, M. Durkin, M. Ibsen, I. Khrushchev, and I. White, Opt. Lett. **23**, 606 (1998).
2. J. J. Yu, G. K. Chang, and O. Akanbi, J. Lightwave Technol. **24**, 271 (2006).
3. J. H. Kim, Y. M. Jhon, Y. T. Byun, S. Lee, D. H. Woo, and S. H. Kim, IEEE Photon. Technol. Lett. **14**, 1436 (2002).
4. D. M. F. Lai, C. H. Kwok, and K. K. Y. Wong, Opt. Express **16**, 18362 (2008).
5. S. E. Kumar, A. E. Willner, D. Gurkan, K. R. Parameswaran, and M. M. Fejer, Opt. Express **14**, 10255 (2006).
6. J. Wang, J. Sun, and Q. Sun, Opt. Lett. **31**, 1711 (2006).
7. J. Qiu, K. Sun, M. Rochette, and L. R. Chen, IEEE Photon. Technol. Lett. **22**, 1199 (2010).
8. J. H. Kim, B. C. Kim, Y. T. Byun, Y. M. Jhon, S. Lee, D. H. Woo, and S. H. Kim, Jpn. J. Appl. Phys. Series **43**, 608 (2004).
9. J. Wang, J. Q. Sun, Q. Z. Sun, D. L. Wang, X. L. Zhang, D. X. Huang, and M. M. Fejer, IEEE Photon. Technol. Lett. **20**, 211 (2008).
10. Y. Fukuchi, M. Akaki, and J. Maeda, IEEE J. Quantum Electron. **41**, 729 (2005).
11. V. G. Ta'eed, N. J. Baker, L. Fu, K. Finsterbusch, M. R. E. Lamont, D. J. Moss, H. C. Nguyen, B. J. Eggleton, D.-Y. Choi, S. Madden, and B. Luther-Davies, Opt. Express **15**, 9205 (2007).
12. M. Pelusi, F. Luan, T. D. Vo, M. R. E. Lamont, S. J. Madden, D. A. Bulla, D.-Y. Choi, B. Luther-Davies, and B. J. Eggleton, Nat. Photon. **3**, 139 (2009).
13. F. Luan, M. D. Pelusi, M. R. E. Lamont, D.-Y. Choi, S. Madden, B. Luther-Davies, and B. J. Eggleton, Opt. Express **17**, 3514 (2009).
14. G. P. Agrawal, *Nonlinear Fiber Optics* (Academic, 2001).
15. X. Gai, S. Madden, D. Y. Choi, D. G. Bulla, and B. Luther-Davies, Opt. Express **18**, 18866 (2010).